



# Least failure energy density: A comprehensive strength index to evaluate and optimize heterogeneous periodic structures

Huawei Feng, Peidong Lei, Huikai Zhang, Bin Liu<sup>\*</sup>

AML, Department of Engineering Mechanics, Tsinghua University, Beijing 100084, PR China

## ARTICLE INFO

### Keywords:

Multiple loading conditions  
Least failure energy density  
Strength  
Topology optimization

## ABSTRACT

Assessing the comprehensive strength of structures under multiple loading conditions is crucial for designing microstructures. This paper proposes the use of the least failure energy density (LFED) to measure the comprehensive strength of heterogeneous periodic structures, which corresponds to the minimum energy density required to destroy a structure. To enhance the comprehensive strength of a periodic structure, the LFED can be maximized. We constructed a two-layer optimization algorithm and found that the high time consumption renders topology optimization unfeasible. We subsequently developed an approach for solving inner-layer optimization analytically and quickly so that the problem becomes a single-layer optimization. We compared the LFED of several classical structures, including plate structures, lattice structures, and TPMSSs. The calculations reveal that plate structures exhibit the best performance in terms of LFED, followed by TPMSSs whereas truss structures have the poorest performance. Among the three types of classical structures, the octet plate, Schwartz-D minimal surface, and octet truss structures are the best-performing types, respectively. Additionally, the LFED is combined with the BESO topology optimization method to obtain the best 2D periodical structure, a 2D curved-edge kagome structure. For optimal 3D periodical structures, rarely discussed space kagome structures (plate or lattice) are obtained with an LFED superior to that of other counterpart classical structures.

## 1. Introduction

Heterogeneous periodic structures have a wide range of applications in different fields, such as the shells of rockets and aircraft (Vasiliev and Razin, 2006), basic structures of construction projects (Ashby, 2006), metamaterials (Zheng et al., 2014), bone materials (Wang et al., 2022), and the microstructures of organisms (Zhang et al., 2020). In recent years, researchers have made significant strides in theoretical and experimental studies of the structural and mechanical properties of periodic structures, such as the effective modulus, bulk modulus (Chatterjee et al., 2021), Young's modulus (Hashin, 1960), shear modulus (Paulino et al., 2009), and stiffness (Berger et al., 2017; Gurtner and Durand, 2014)), Poisson's ratio (Sigmund, 2000; Watts and Tortorelli, 2017), and specific strength (Bauer et al., 2014). In these studies, microstructures assembled from lattices (Deshpande et al., 2001; Hanks et al., 2020; Helou and Kara, 2018; Pan et al., 2020), plates (Berger et al., 2017), and triply periodic minimal surfaces (TPMSSs) (Al-Ketan et al., 2020; Bonatti and Mohr, 2019). However, research on the comprehensive strength of microstructures under complex multiple loading conditions has not been adequately addressed.

\* Corresponding author.

E-mail address: [liubin@tsinghua.edu.cn](mailto:liubin@tsinghua.edu.cn) (B. Liu).

For conventional materials, the future loading conditions are uncertain, and it is important to ensure that the lower limit of the strength of these materials is sufficiently high in the design. Multiple complex loading conditions, such as walking, running, and jumping, can lead to the formation of a porous trabecular bone topology, enabling the microstructure of a skeleton to meet strength requirements under varying conditions (Zhou and Sigmund, 2017). In the design of automotive chassis skeletons, factors such as static loads, tilts, and hill climb need to be considered, with each skeleton topology requiring compliance with specified strength indices (Cui et al., 2022). As the number of loading conditions increases, defining a reasonable strength index as an optimization objective becomes a challenging problem. Using a statistical approach, a weighted-strength optimization objective (Atwal et al., 2012) is proposed on the basis of the probability distribution of random loading conditions. However, this approach does not guarantee the ability of a structure to withstand external mechanical loads under every loading condition. From the perspective of strength anisotropy, Messner (2016) employed the maximum cylindrical deviation from the volumetric axis of the principal stress space as an index to optimize periodic truss structures. However, this measurement imposes a strength requirement in a particular direction in the stress space, and the resulting optimization problem is not frame invariant. Furthermore, Coelho et al. (2021) attempted to minimize the maximal von Mises stress in porous composite microstructures via shape and topology optimization. However, these scholars optimized only the shape of the hole and did not extend to the more general case of topological optimization.

Therefore, in this paper, a well-defined index with practical physical meaning is proposed to characterize the comprehensive strength of a heterogeneous periodic structure. This paper is structured as follows: Section 2 introduces the proposed comprehensive strength measure, the least failure energy density (LFED), for measuring the strength of periodic structures and materials under complex multiple loading conditions. In Sections 3 and 4, we investigate the optimal truss structures and topology optimization structures, respectively, on the basis of the LFED. The optimization of beams and plates, which represent periodic structures subjected to nonperiodic loads, is discussed in Section 5. The conclusions and discussion are given in Section 6.

## 2. Definition of a comprehensive strength measure — least failure energy density

To propose an objective index with practical physical meaning to characterize the comprehensive strength of a heterogeneous periodic structure, it is necessary to address the strength weaknesses of the structure. Such weaknesses cannot be accurately determined by simply superimposing the strengths of a finite number of loading conditions. Therefore, we introduce the following definition:

$$\begin{aligned} \text{Least Failure Energy Density (LFED)} : \quad & \text{LFED} = \min_{\bar{\sigma}} \frac{1}{2} \bar{\sigma} \bar{e} \\ & \text{st : } f(\bar{\sigma}) = 0 \end{aligned} \quad (1)$$

In Eq. (1),  $\bar{\sigma}$  and  $\bar{e}$  denote the overall effective stresses and effective strains within the representative volume element (RVE), respectively.  $\frac{1}{2} \bar{\sigma} \bar{e}$  represents the average strain energy density of the RVE, and  $\bar{\sigma} = [\bar{\sigma}_x, \bar{\sigma}_y, \bar{\sigma}_z, \bar{\tau}_{yz}, \bar{\tau}_{xz}, \bar{\tau}_{xy}]$  also represents the loading space of the RVE. The failure surface in terms of effective stress is denoted by  $f(\bar{\sigma}) = 0$  and depends on the mechanical properties of the constituent materials and their microstructures. Eq. (1) implies that, after the RVE undergoes all possible deformations under various loading conditions, the least strain energy density required to cause failure is determined. Therefore, if the strain energy density of the RVE is lower than the corresponding LFED, then the periodic structure is considered safe.

The LFED of a structure is an important indicator of its safety, as a higher value implies a lower likelihood of failure. Thus, the LFED should be optimized in the design of microstructures. The optimization goal is to continuously improve the lower bound of the structure's strength, thereby minimizing its "weak points." Consequently, the LFED reflects a structure's "weak point" under various complex loadings. A structure with a sufficiently strong "weak point" implies that, regardless of the loading combination (including compression, shear, bending, and torsion), it will not easily fail. Therefore, it can be considered a structure with excellent overall strength performance under complex load conditions.

The question of whether LFED or von Mises stress is more suitable for measuring heterogeneous periodic structures is a topic worth exploring. Von Mises stress reflects only the deviatoric energy, which is the energy associated with shape change. It does not account

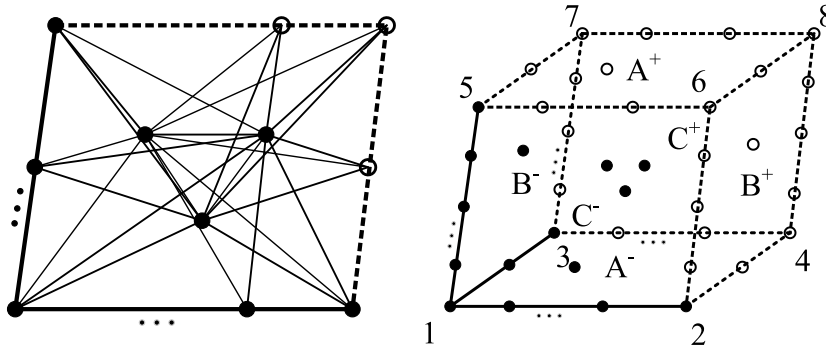


Fig. 1. 2D and 3D truss structures to be optimized.

for hydrostatic stress components, as hydrostatic stress in a homogeneously distributed solid medium does not lead to material failure. However, in heterogeneous periodic structures—characterized by numerous voids and spatial configurations—hydrostatic stress can indeed cause failure. Strain energy density, however, effectively accounts for both deviatoric energy and deformation energy in the hydrostatic loading, making it a more suitable measure for assessing the strength of such heterogeneous structures.

In the following sections, we first explore the optimal truss structures and discuss their optimized upper bounds. Then we perform topological optimization of the periodical structure and compare the optimized results with classical structures.

### 3. Truss structures with optimal least failure energy density

We initially investigate the optimization of truss structures. We improve the LFED by optimizing the node positions and the cross-sectional areas of the struts.

**Fig. 1** shows the initial structure to be optimized. We introduce several random nodes and connecting struts within the parallelogram RVE to maximize the LFED of this structure through the optimization of the node locations and the cross-sectional areas of the struts. The material has a Young's modulus of  $E$  and a volume fraction of  $\bar{\rho}$ , and the struts have critical failure stresses of  $\sigma_c$ .  $f(\bar{\sigma}) = 0$  corresponds to the situation in which the maximum stress in the rods of the RVE just reaches the threshold of failure  $\sigma_c$ . The expression of the optimization is shown as follows:

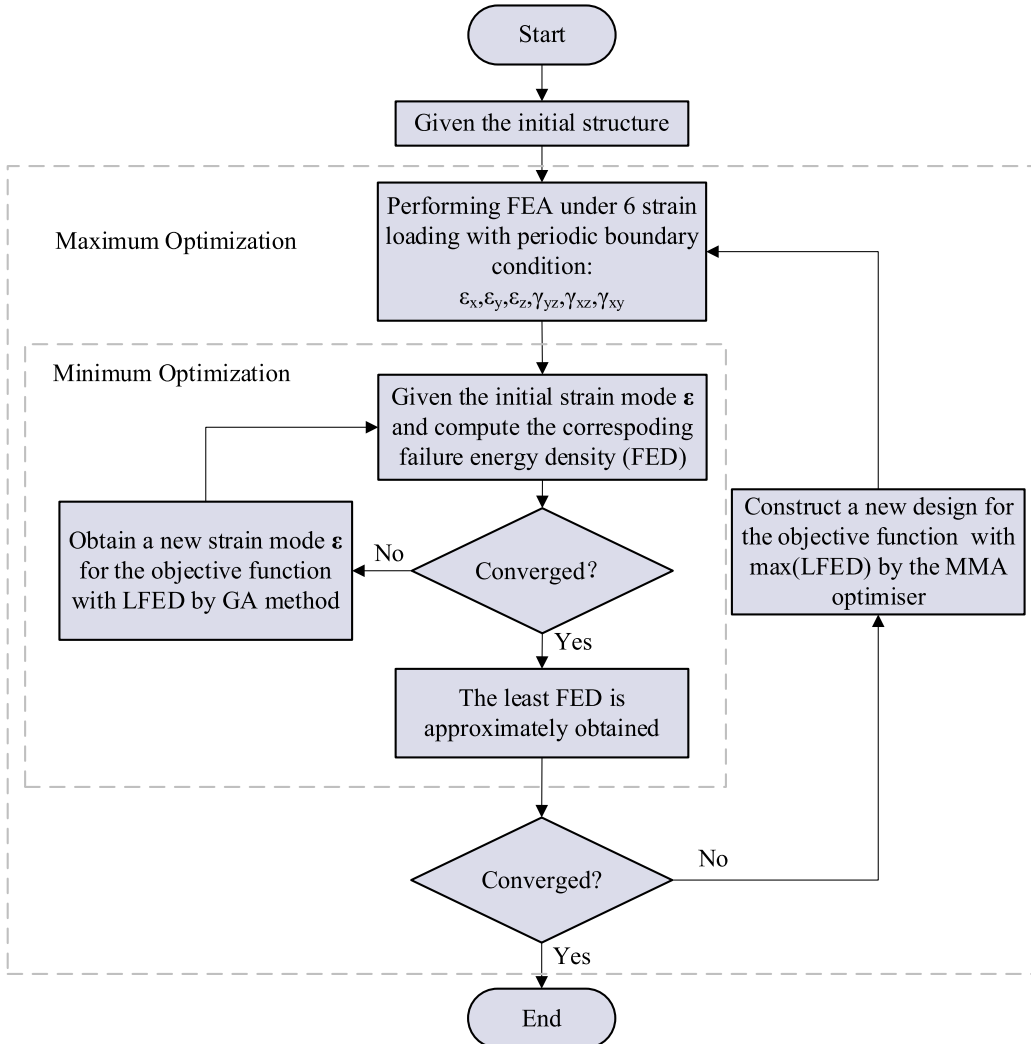


**Fig. 2.** Flow chart of the optimization of truss structures.

$$\max_{x,A} \text{LFED} = \max_{x,A} \left\{ \begin{array}{l} \min_{\bar{\sigma}} \frac{1}{2} \bar{\sigma} \epsilon \\ \text{st : } f(\bar{\sigma}) = 0 \\ \text{st : } \rho = \bar{\rho} \end{array} \right\} \quad (2)$$

where  $x$  is the coordinate of the nodes and  $A$  is the cross-sectional area of the struts. The flow chart of the algorithm, which consists of a two-layer optimization problem, is shown in Fig. 2. The inner layer involves a minimum optimization problem, which aims to determine the least energy density required to destroy a specific structure by traversing all possible deformations, i.e., LFED. The outer layer is a maximum optimization problem that aims to design a structure with the maximum LFED by changing the structural parameters under the same volume fraction.

To accelerate the calculation process, two strategies are adopted. First, by calculating 6 basic strains in 3D problems (or 3 basic strains in 2D problems) via finite element simulations, linear combinations of these cases can then be used for the finite element analysis of other scenarios, thereby significantly reducing the inner optimization computation time to approximately 3 s via the genetic algorithm (GA). Second, the method of moving asymptotes (MMA) is used for parameter optimization at the maximum optimization problem layer (or outer layer), and the sensitivity can be calculated via differencing because of the small number of optimization variables.

The optimization process yields three optimal plane truss structures, as shown in Fig. 3, all of which have LFEDs of  $\frac{1}{6}\rho \frac{\sigma_c^2}{E}$ . These findings indicate that these structures require a least energy density of  $\frac{1}{6}\rho \frac{\sigma_c^2}{E}$  to damage any of the struts. A discussion of this theoretical upper limit is presented in the Appendix. (See Appendix)

Similar to the optimization for planar trusses, we obtain four optimal 3D truss structures in Fig. 4, whose LFED values are  $\frac{1}{12}\rho \frac{\sigma_c^2}{E}$ , which correspond to the strength safety limit of the spatial truss structure.

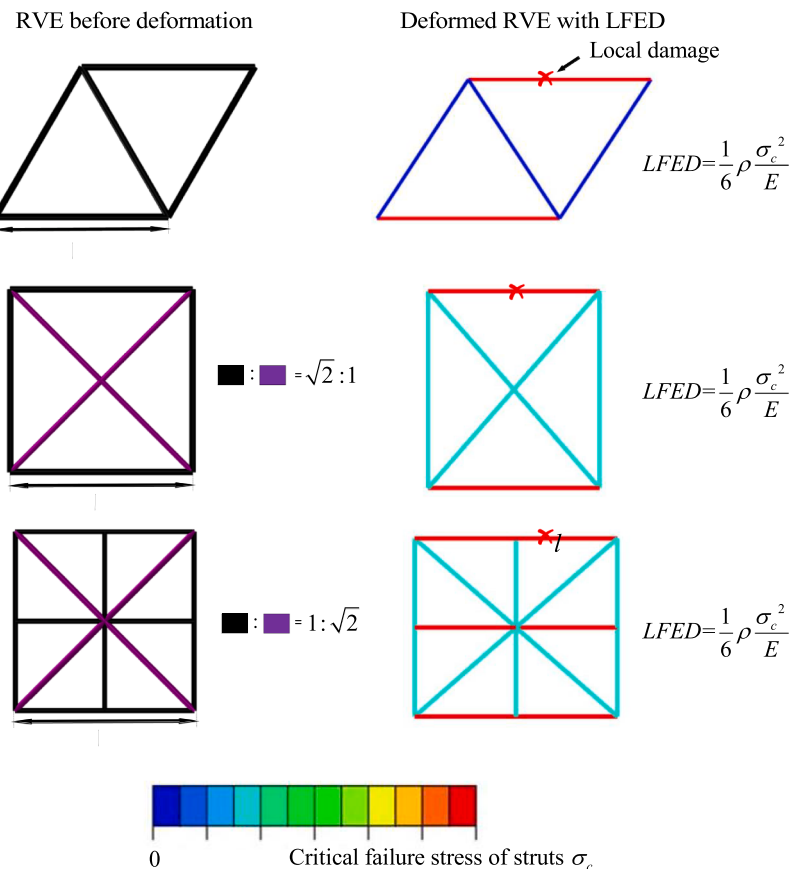


**Fig. 3.** Optimization results of planar truss structures. (The ratio represents the cross-sectional area ratio of different struts.).

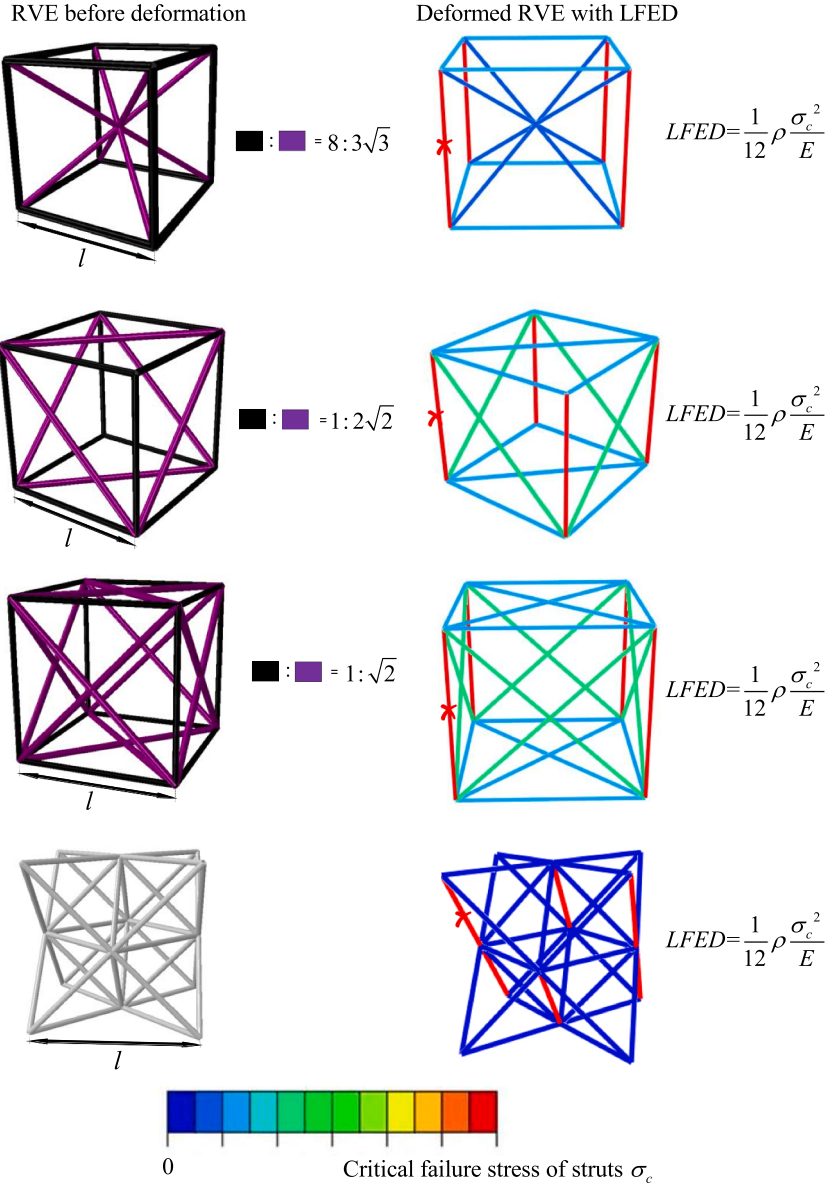


Fig. 4. Optimization results of spatial truss structures.

#### 4. Topology optimization method based on LFED

In the previous section, we explore truss structures with the optimized LFED. However, in real-world engineering applications, the local components of these structures are often subjected to complex deformations such as bending and torsion, and damage typically occurs at the connecting nodes rather than in the middle of the struts. Therefore, to account for these more general situations, we employ topology optimization via the bidirectional evolutionary structural optimization (BESO) method (Cui et al., 2022) combined with the LFED to design periodic heterogeneous solid structures with higher comprehensive strength. The optimization problem is formulated in Eq. (3):

$$\max_x \left\{ \min_{\bar{\sigma}} \frac{1}{2} \bar{\sigma} \epsilon \right\} \\ \text{st} : f(\bar{\sigma}) = 0 \\ \text{st} : \rho = \bar{\rho} \\ x = x_{\min} \text{ or } 1 \quad (3)$$

where  $\mathbf{x}$  represents the density variable of the pixel elements and  $\rho$  is the volume fraction. For topology optimization, the local von Mises stress  $\sigma_{\text{mises}}^{\text{local}}$  is used to determine failure if  $\max(\sigma_{\text{mises}}^{\text{local}}) \geq \sigma_c$ .

The algorithm incorporates two types of optimization possibilities: topology optimization of a specific RVE shape and affine transformation of the RVE into arbitrary parallelograms in the plane and parallel hexahedra in space.

#### 4.1. An approach for computing the LFED efficiently to transform a two-layer optimization process into a single-layer optimization process

The typical topology optimization method is based on a pixel description and therefore has many more optimization variables than the truss structure does. If a  $60 \times 60 \times 60$  grid is used as the optimization variable, then a direct two-layer optimization computation would take approximately 10 years on the basis of our initial trial simulations. Since the sensitivity calculation takes 1.5 s per element and the overall prediction is 1000 iterations,  $1.5 \times 60^3 \times 1000 \text{ seconds} \approx 10.27 \text{ years}$ . However, if it can be transformed into a single-level optimization, then the time required can be significantly reduced. Therefore, it is necessary to solve the inner optimization problem analytically.

In the following derivation, variables with a line ‘-’ refer to the quantities of the RVE, whereas variables with a superscript ‘local’ refer to the elements. The core idea of the calculation for the  $i^{\text{th}}$  element in the 2D problem is schematically shown in Fig. 5 over the loading space  $\bar{\sigma} = [\bar{\sigma}_{11} \quad \bar{\sigma}_{22} \quad \bar{\sigma}_{12}]^T$  of the RVE. For all possible loadings on the RVE with an isoenergy density of a specific value, an isoenergy density surface is plotted in Fig. 5 to represent the loading surface, and its shape is an ellipsoid because the energy density  $U$  has the following quadratic form:

$$U = \frac{1}{2} \bar{\sigma}^T \mathbf{S}_{\text{eff}} \bar{\sigma} \quad (4)$$

where  $\mathbf{S}_{\text{eff}}$  is the compliance matrix of the RVE.

The failure criterion of the  $i^{\text{th}}$  element is assumed to be the following:

$$f^{local}(\sigma^{\text{local}}) = 0 \quad (5)$$

where  $\sigma^{\text{local}} = [\sigma_{11}^{\text{local}} \quad \sigma_{22}^{\text{local}} \quad \sigma_{12}^{\text{local}}]^T$  is the stress of the element. From 3 finite element analyses under 3 independent stress loads with periodic boundary conditions, the following linear relationship between  $\bar{\sigma}$  and  $\sigma^{\text{local}}$  is obtained:

$$\sigma^{\text{local}} = \mathbf{N} \bar{\sigma} \quad (6)$$

where  $\mathbf{N}$  is the coefficient matrix, which has different values for different elements. Substituting Eq. (6) into Eq. (5) yields the failure surface of the  $i^{\text{th}}$  element in terms of  $\bar{\sigma}$ :

$$f^{local}(\mathbf{N} \bar{\sigma}) = 0 \quad (7)$$

which is also plotted in Fig. 5.

As the loading surface increases, the LFED can be determined when the first point in an element touches the failure surface, indicating the failure of the element and the RVE structure. Specifically, the first point to be touched is the one with the smallest radius ratio  $\min \frac{r_{\text{failure-surface}}}{r_{\text{energy-density}}}$  between the failure surface and the loading surface (Fig. 5). We search for its minimum value over all the elements, and the most dangerous element and the LFED of the RVE can be determined.

For some simple failure criteria, the calculation can be very fast. Using the following von Mises failure criterion as an example,

$$f^{local}(\sigma^{\text{local}}) = (\sigma_{11}^{\text{local}})^2 + (\sigma_{22}^{\text{local}})^2 - \sigma_{11}^{\text{local}} \sigma_{22}^{\text{local}} + 3(\sigma_{12}^{\text{local}})^2 - \sigma_c^2 = 0 \quad (8)$$

It can also be expressed in matrix form as follows:

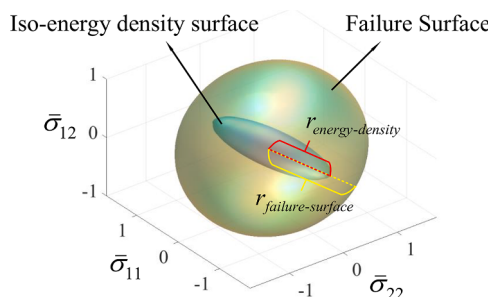


**Fig. 5.** Schematic diagram of the calculation method of the LFED for 2D problems.

$$f^{local}(\sigma^{local}) = \sigma^{local T} M \sigma^{local} - \sigma_c^2 = 0 \quad (9)$$

where

$$M = \frac{1}{2} \begin{bmatrix} 2 & -1 & 0 \\ -1 & 2 & 0 \\ 0 & 0 & 6 \end{bmatrix} \quad (10)$$

Substituting Eq. (6) into Eq. (9) yields the failure surface in terms of  $\bar{\sigma}$ :

$$f^{local}(N\bar{\sigma}) = \bar{\sigma}^T N^T M N \bar{\sigma} - \sigma_c^2 = 0 \quad (11)$$

We now have two ellipsoidal functions: the isoenergy density ellipsoid corresponding to the matrix  $\frac{1}{2}S_{eff}$  and the von Mises failure surface ellipsoid corresponding to the matrix  $N^T M N$ . We map the two ellipsoids simultaneously via an affine transformation to transform the isoenergy density ellipsoid into a sphere in the mapping space of  $\tilde{\sigma} = L^T \bar{\sigma}$ , where  $L$  is the transformation matrix satisfying  $\frac{1}{2}S_{eff} = LL^T$ . The corresponding matrix of the von Mises failure surface ellipsoid after the affine transformation is  $L N^T M N L^T$ . From the knowledge of linear algebra, the lengths of each axis of the ellipsoid are equivalent to the eigenvalues of the corresponding ellipsoid

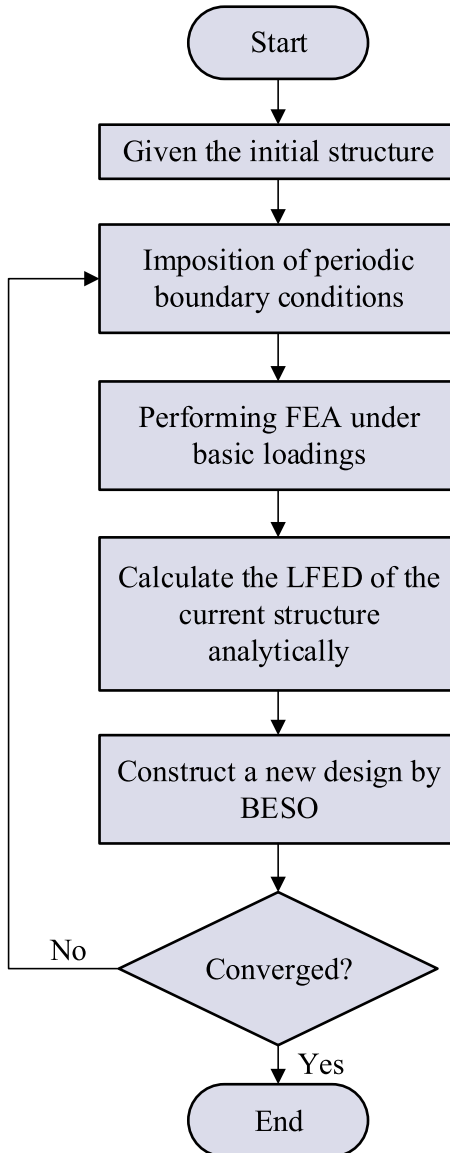


Fig. 6. Topology optimization flow chart based on the LFED.

matrix. Thus, the problem reduces to finding the minimum eigenvalue of  $\mathbf{LN}^T \mathbf{MNL}^T$ . That is,  $\min[\text{eig}(\mathbf{LN}^T \mathbf{MNL}^T)]$  corresponds to the energy density required to destroy the  $i^{th}$  element. By searching over all the elements, the least energy density required to destroy the RVE, i.e., LFED, can be obtained.

Notably, in the above derivation, the material is assumed to be linear elastic. Obviously, the approach can be easily extended to other cases, such as 3D problems, and a structure under more loadings. The flowchart of single-layer optimization is shown in Fig. 6.

#### 4.2. Numerical examples of 2D topology optimization based on the LFED

We constrain the volume fraction to  $\rho=50\%$ . By varying the initial configuration (e.g., using various combinations of orthogonal polygons), iteration rate, and RVE shape, we have optimized several optimal structures. The configurations of these structures, along with the von Mises stress contours when they are destroyed with the lowest energy density, are presented in Fig. 7. The red regions represent the local failure region of the structure. Our results indicate that the curved-edge kagome structure is the best among the 2D structures. This structure has an LFED value of  $0.0497 \frac{\sigma_c^2}{E}$ , where  $E$  is the Young's modulus.

In addition, we have also investigated the LFED for these structures when the volume fraction varies from 20 % to 50 %, as shown in

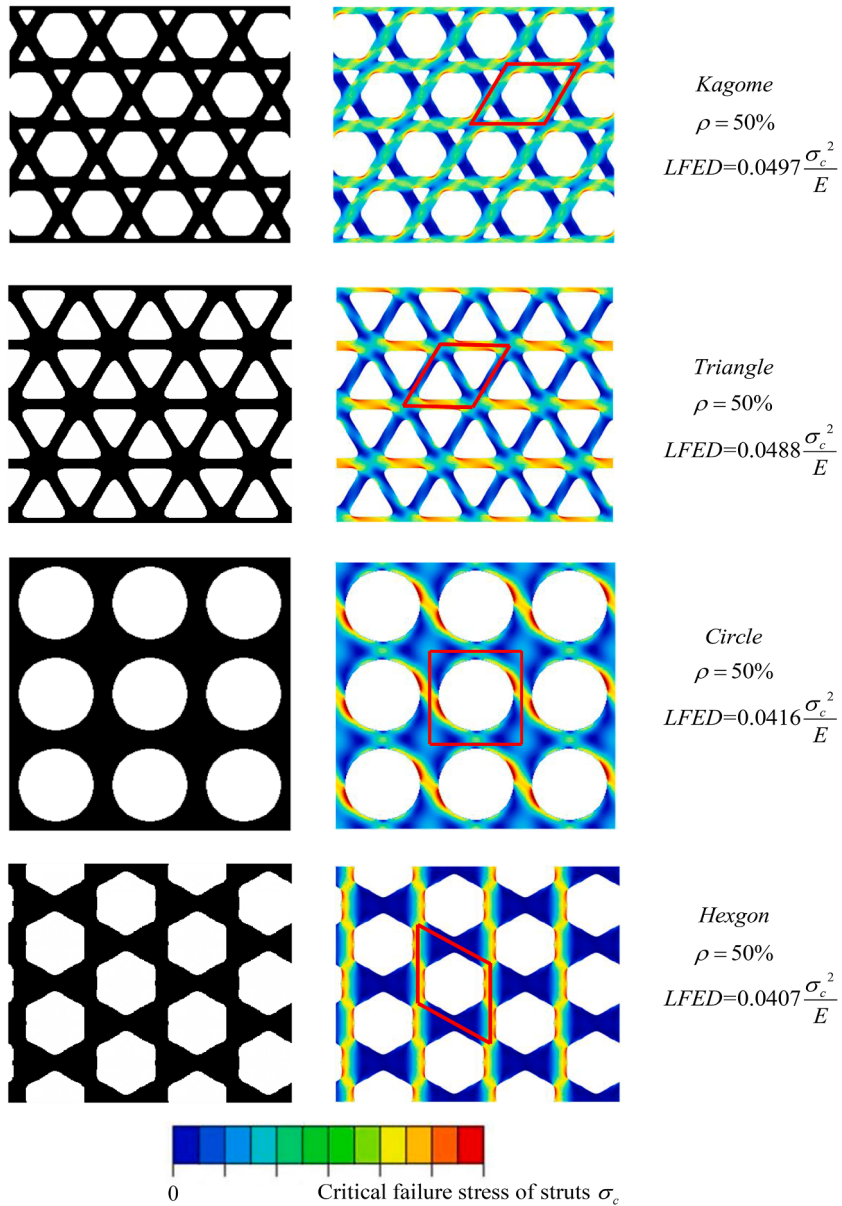


Fig. 7. Topology optimization results of 2D structures based on the LFED.

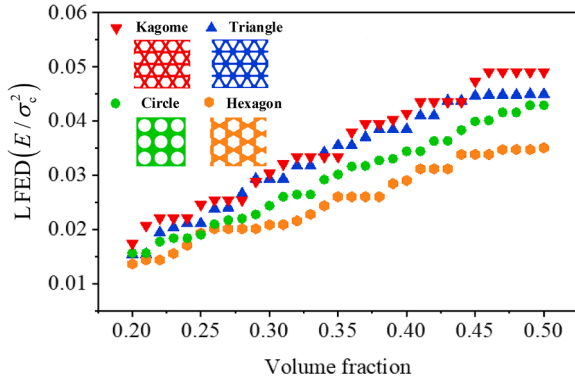


Fig. 8. LFED versus volume fraction for various 2D structures.

Fig. 8, which indicates that the kagome structure remains the optimal choice for all volume fractions. This finding is consistent with the results of previous studies, thus justifying the rationality of the LFED index. A question attracting more attention is as follows: what is the optimal structure in three dimensions?

Table 1

Comparison of LFEDs for classical 3D structures, categorized by plate structure, lattice structure, and TPMS.

Plate	Octet	BCC+FCC	SC	Octet+SC
Sketch				
$LFED\left(\frac{\sigma_c^2}{E}\right)$	0.11530	0.11334	0.06153	0.02932
Lattice	Octet	BCC	BCC+FCC	FCC
Sketch				
$LFED\left(\frac{\sigma_c^2}{E}\right)$	0.035975	0.02857	0.02608	0.02019
TPMS	Schwarts-D	Schwarts-P	Schoen-Gyroid	Neovius
Sketch				
$LFED\left(\frac{\sigma_c^2}{E}\right)$	0.05069	0.04275	0.03185	0.03021

All the above structures meet:  $\nu=0.3$ ,  $\rho=20\%$ , Mesh:  $50 \times 50 \times 50$ .

#### 4.3. 3D topology optimization based on LFED

Before searching for the optimal 3D structure, we first evaluate the performance of widely known classical structures, including plate structures, truss structures, and TPMS. We use the same mesh division, material, and volume fraction constraints for each structure. The results are summarized in [Table 1](#).

According to [Table 1](#), the plate structures outperform the other two classical structures with the maximum LFED. The TPMS structures come in second, while the truss structures have the worst performance. Among the three types of classical structures, the octet plate, Schwartz-D minimal surface, and octet truss exhibit the best performance.

Next, we attempt to design a structure with a better LFED via topology optimization. In the initial step of optimization, we hollow out the middlemost element of the cube to break the equilibrium. [Fig. 9](#) shows the optimization process, where only half of the profile is shown to display the internal structure more clearly. At the 130th iteration, the optimized structure appears as a combination of an outer plate structure and an inner complex truss structure. As the volume fraction continues to decrease, the inner truss structure gradually disappears, and at the 161st iteration, it forms a varying thickness perforated plate structure similar to the SC plate. This optimal structure is obtained under the cubic RVE and has an LFED value of 0.13097, surpassing all previously known classical structures.

Next, we introduce the affine transformation of the RVE to the optimization algorithm so that the search space is not limited to the cube but can also include all parallel hexahedra.

[Fig. 10](#) displays the optimal structure from the optimization after introducing the affine transformation; this structure is referred to as the space kagome plate structure. There are four cross sections with different orientations showing 2D kagome structures. The RVE of a space kagome consists of four parts, namely, two ortho-tetrahedral plates and two polyhedrons consisting of a combination of ortho-triangular and ortho-hexagonal plates, as shown in [Fig. 10\(b\)](#). A cross-sectional view of the interior of this structure is presented in [Fig. 10\(a\)](#). [Fig. 10\(c\)](#) and [10\(d\)](#) show the internal cross section of the optimization process. The LFED of such a space kagome plate structure is  $0.14650\frac{c^2}{E}$  for a 20 % volume fraction. It is the optimal structure based on the LFED in three dimensions, which is consistent with the optimization results in two dimensions.

Moreover, from the curves of the LFED with varying volume fractions in [Fig. 11](#), the space kagome structure is optimal when the volume fraction is approximately 20 %, whereas the orthorhombic RVE achieves better performance at higher volume fractions. This conclusion might be slightly affected by the mesh density due to the limitation of simulation capacity.

In addition, Norman A Fleck ([Symons et al., 2004](#)) proposed a kagome double-layered grid with only one orientation showing a 2D kagome cross section, which is different from the space kagome structure in geometry. To compare their mechanical properties, we calculate the LFED of various lattice models with different volume fractions. [Fig. 12](#) shows that the LFED of the space kagome lattice is always greater than that of the kagome double-layered grid, which further reflects the rationality of the space kagome design. In addition, both the space Kagome lattice structure and the octet structure achieve superior values. In an octet lattice structure, each node has 12 connecting struts in 6 directions, whereas in a space-Kagome lattice structure, each node has 6 connecting struts in 3 directions. For a given volume fraction, the aspect ratio of connecting rods in the space Kagome lattice structure is half of that of the octet structure. Thicker rods means that the structure is more resistant to buckling. Fewer connecting rods per node results in less risk of stress concentration at the nodes because of the larger angles among rods.

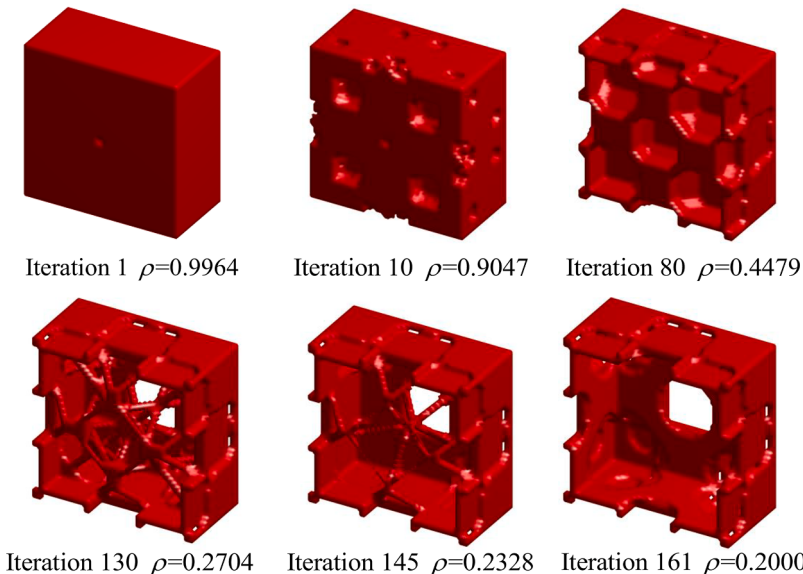


[Fig. 9](#). Topology optimization results for a 3D structure with a filter.

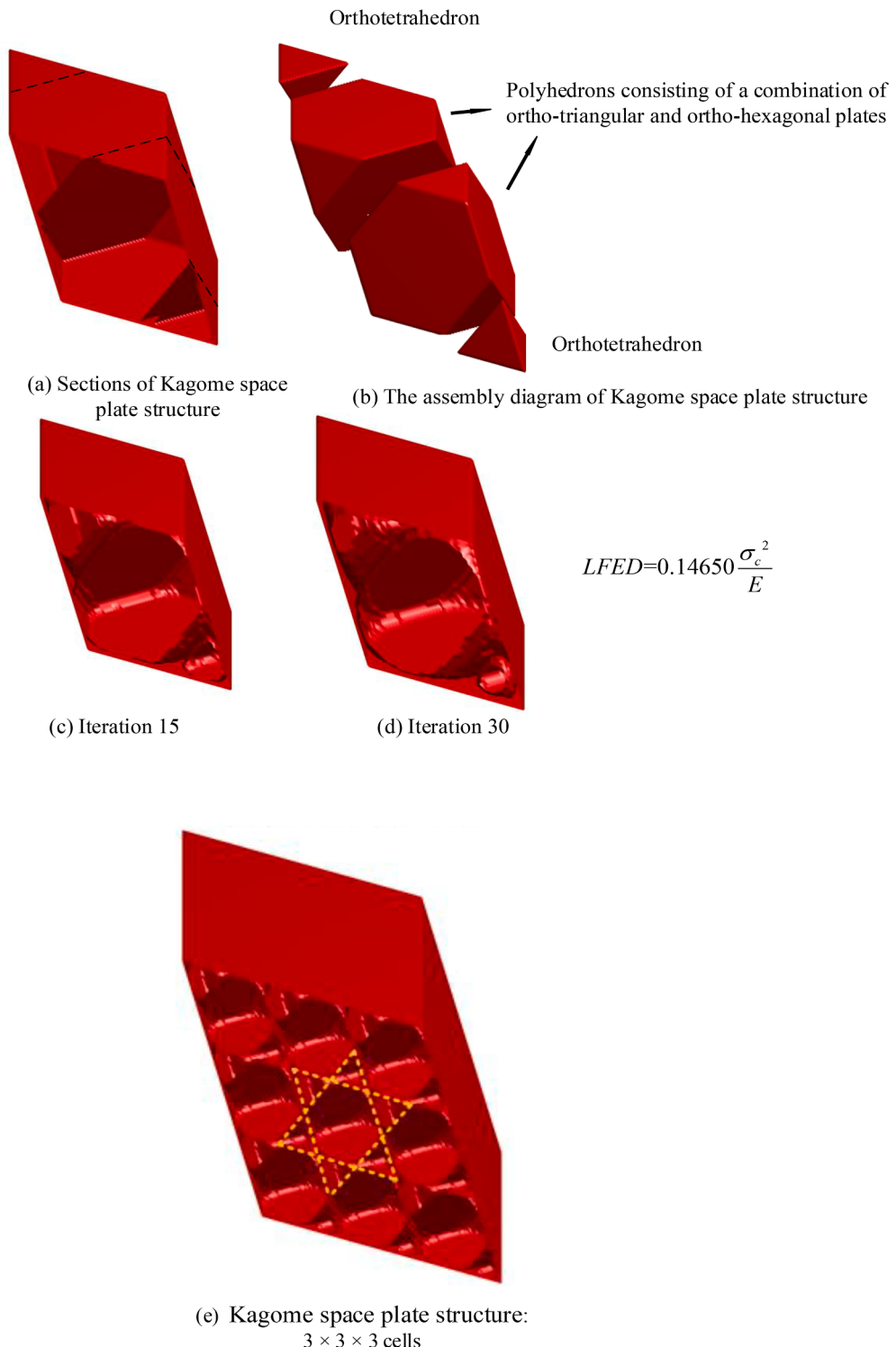


**Fig. 10.** Three-dimensional structure with the optimal LFED-space kagome plate.

##### 5. Application of LFED-based optimization to periodic structures subjected to nonperiodic loads: optimization of beams and plates

The above work focuses on structural optimization under periodic loading, and next, we attempt to broaden the application of the

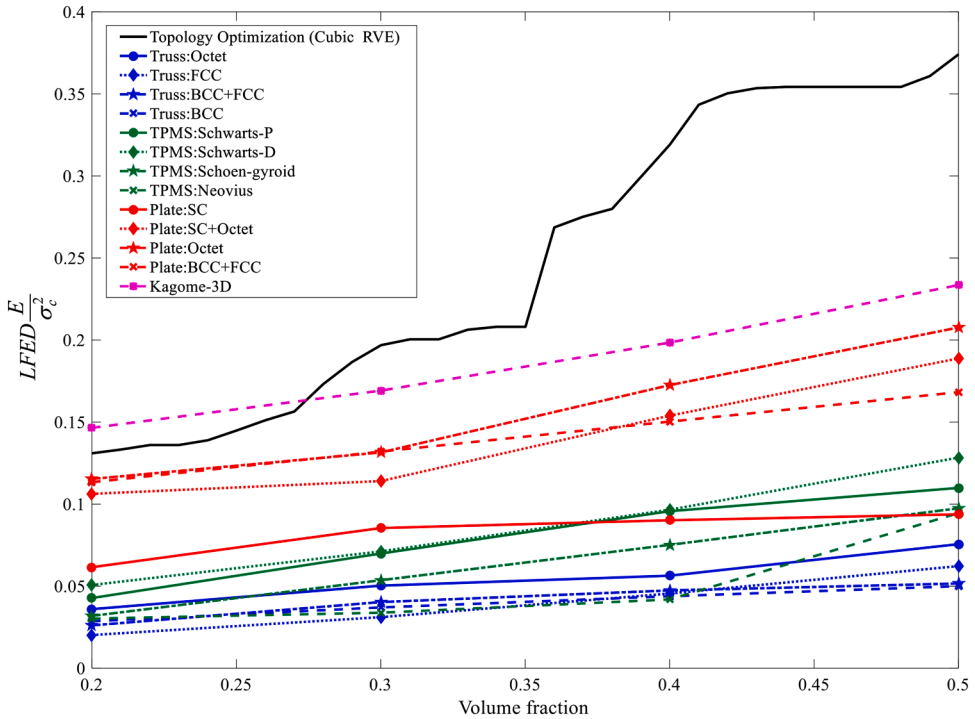


**Fig. 11.** Curves of the LFED versus volume fraction for 3D structures during optimization.

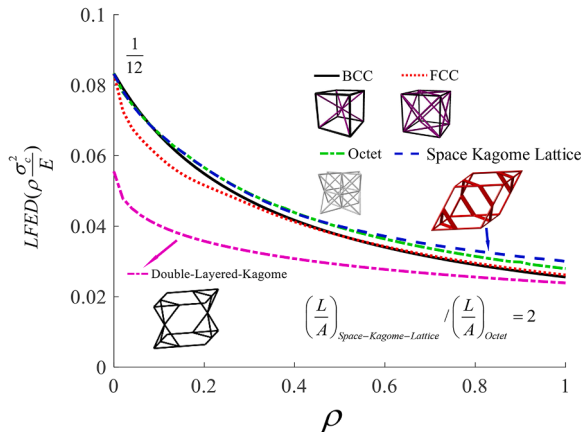


**Fig. 12.** LFED versus volume fraction for various 3D lattices.

LFED to beam and plate structures to address nonperiodic deformations such as bending and torsion. For periodical structures under periodical loading, all unit cells undergo identical deformation. The effective stress/strain method is a basic loading protocol. For nonperiodical loadings, one of the most dangerous loadings is a concentrated force, but it is not a common scenario and lacks research significance. To exclude such extreme loading cases, a reasonable load should be applied from a distant location, i.e., remote loading. Therefore, we investigate only the failure of the centered unit cell and compute its LFED.

### 5.1. Application of the LFED to optimize the topology of beam structures

Given the uncertainty of loads on a beam, determining the optimal comprehensive strength for designing the safest, most reliable, and least prone-to-failure beam merits thorough investigation. The beam is usually subjected to four basic types of loads, such as tension, shear, bending, and torsion, where shear and bending have two loading modes each along the x-direction and y-direction, which means that there are six basic loading modes, as shown in Fig. 13. Thus, the problem can be described as follows: to possess the maximum LFED when subjected to an infinite combination of these six basic loads, what is the structural design of the beam? We use

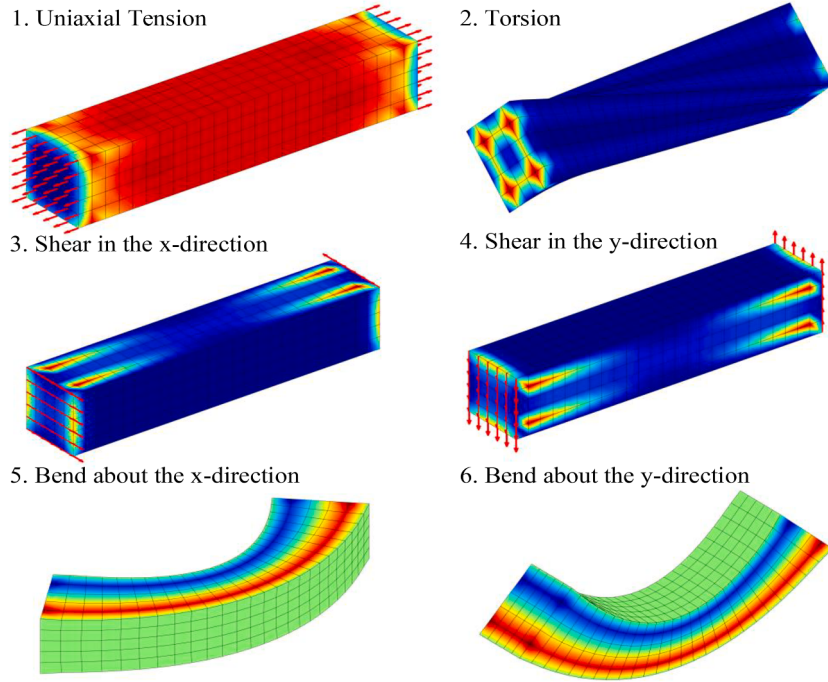


**Fig. 13.** Basic loading modes for a beam.

the 9:1:1 rectangular beam structure in Fig. 14 as the design domain for optimization. The optimization results in a cylinder of uniform thickness, which agrees with the optimal beam structure, as per our experience.

### 5.2. Application of the LFED to the optimal design of plate structures

The LFED can also be employed to investigate the comprehensive strength of a periodic plate structure. The plate is usually subjected to five types of basic loads, i.e., tensile, compression, shear, bending and torsion. Here, tensile, bending and torsion loads have two loading modes each along the x-direction and y-direction, which means that there are 10 basic loading modes, as shown in Fig. 15. Similar to the problem described above: to have the maximum LFED when subjected to an infinite combination of these ten basic loads, what is the structural design of the plate?

It should be pointed out that the previous analytical approach is still applicable for cases with >6 basic loadings. Assuming that  $\mathbf{F}$  is the matrix of basic loadings, similar to  $\bar{\sigma}$  in Eq. (6), the local stress has a linear relation with the loading as follows:

$$\boldsymbol{\sigma}^{\text{local}} = \mathbf{N}\mathbf{F} \quad (12)$$

The energy density can be expressed as:



**Fig. 14.** Topology optimization results for a beam.

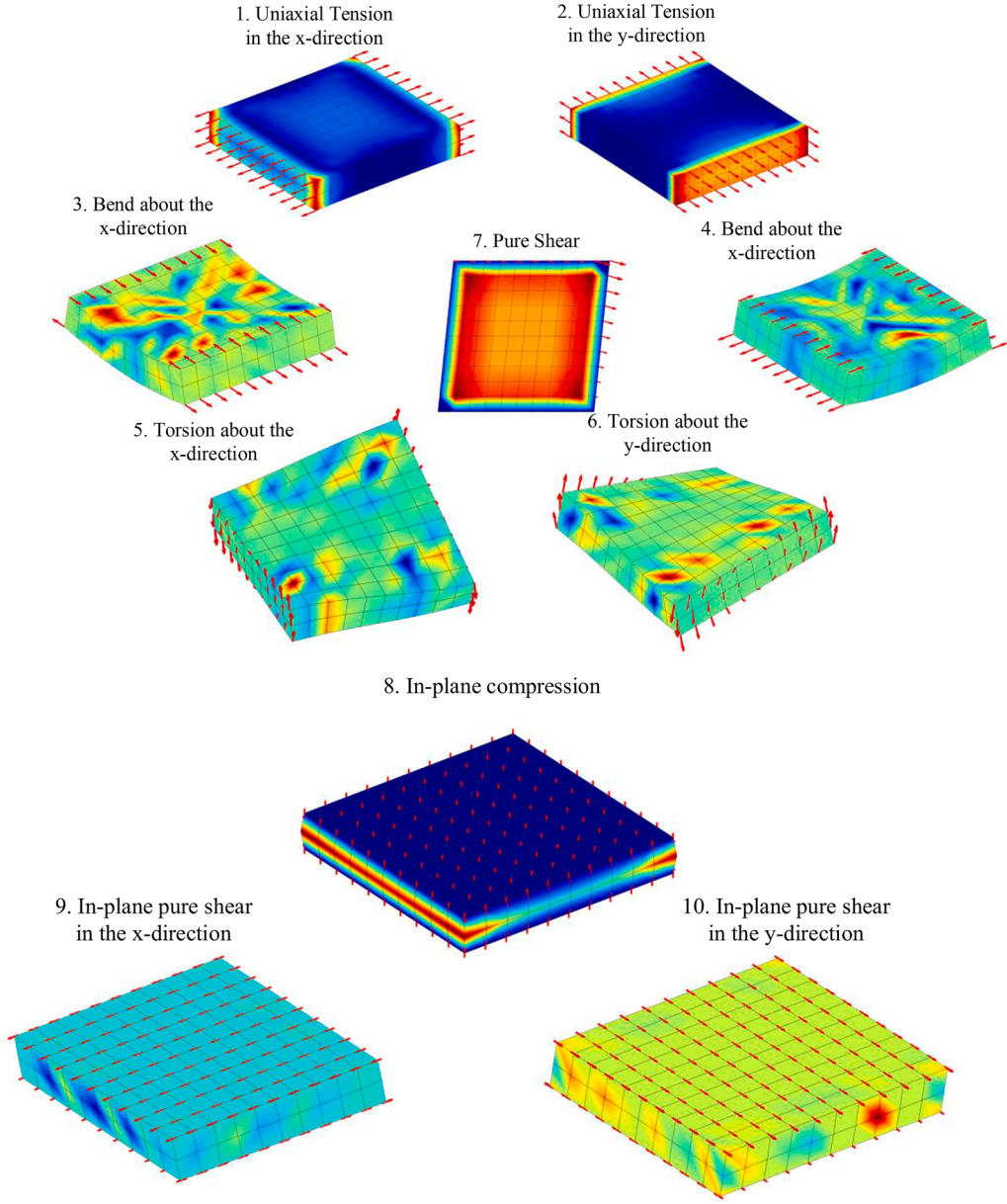


**Fig. 15.** Basic loading modes for a plate.

$$U = \frac{1}{2V} \int_V \sigma^{\text{local}} \mathbf{S}^{\text{local}} \sigma^{\text{local}} dV = \frac{1}{2} \mathbf{F}^T \left( \frac{1}{V} \int_V \mathbf{N}^T \mathbf{S}^{\text{local}} \mathbf{N} dV \right) \mathbf{F} \quad (13)$$

$\frac{1}{V} \int_V \mathbf{N}^T \mathbf{S}^{\text{local}} \mathbf{N} dV$  is similar to  $\mathbf{S}_{\text{eff}}$  in Eq. (4). The remainder of the derivation remains the same.

We obtain the optimal plate structure in Fig. 16. The left topology result shows the optimized structure, which is a sandwich-like structure with a middle stiffened layer. The right is a cross-sectional view where the details of the internal stiffening can be seen.

### 5.3. Optimization for comprehensive strength and comprehensive stiffness

As discussed above, the LFED can be used as an index to evaluate and optimize the comprehensive strength. However, in some cases, as presented later in this section, optimizing the LFED may result in a low-stiffness structure. Therefore, both the comprehensive strength and comprehensive stiffness should be optimized simultaneously in this case. One question arises first: how can a comprehensive stiffness index be defined?

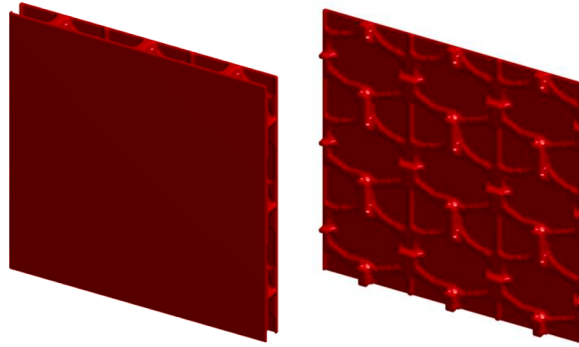


**Fig. 16.** Topology optimization results for plate structures.

We use the following example to discuss these issues. A tower crane structure is a commonly adopted periodic truss structure that can withstand complex compression, shear, bending, torsion and other loads during operation, and at the same time, the design needs space for the staff to climb upward. The mainstream design structure is shown in Fig. 17.

Using the LFED as the single optimization index, we first optimize the cross-sectional area of the rod. The optimized structure with the maximum comprehensive strength is shown in Fig. 18a, which unfortunately has very low stiffness.

The stiffness also plays an important role in safe design. For the optimization of the comprehensive stiffness, we adopt the minimum eigenvalue of the stiffness matrix as an optimization indicator. A larger minimum eigenvalue of the stiffness matrix means that the structure will be less deformed under various loads. The optimized structure with the maximum comprehensive stiffness is shown in Fig. 18b.

The different magnitudes of strength and stiffness present a significant challenge for joint optimization. A feasible method is proposed to address this issue as follows. Initially, separate optimizations for strength and stiffness are performed on the basis of the optimal LFED and the optimal minimum eigenvalue of the stiffness matrix, respectively. We then obtain the upper bounds of the LFED ( $LFED_{upper-bound}$ ) and the upper bounds of the minimum eigenvalue of the stiffness matrix ( $min-eigenvalue_{upper-bound}$ ). The combined optimization objective is subsequently defined as  $\max(LFED / LFED_{upper-bound}, min-eigenvalue / min-eigenvalue_{upper-bound})$ . This objective promotes the optimization of the stiffness when the strength ratio is high and the optimization of the strength when the stiffness ratio is high, thus facilitating joint synergistic optimization.

The result for the synergistic optimization of the comprehensive strength and comprehensive stiffness is depicted in Fig. 18c. For the optimal structure, both the LFED and the minimum eigenvalue of the stiffness matrix reach 0.9565 of their upper bounds. This indicates that the structure is a Pareto optimal solution for this optimization problem, meaning that any modifications to the structure will result in a decrease in either stiffness or strength. Therefore, this structure exhibits excellent performance in terms of both strength and stiffness, potentially providing valuable insights for the future design of tower crane structures.

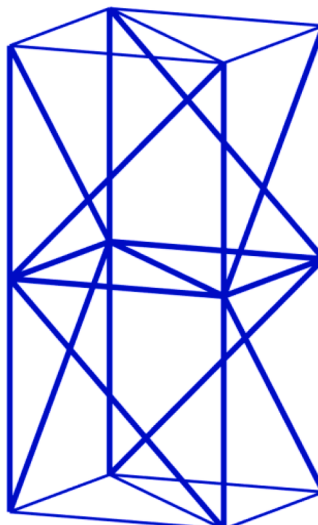


**Fig. 17.** Unit cell of a tower crane structure.

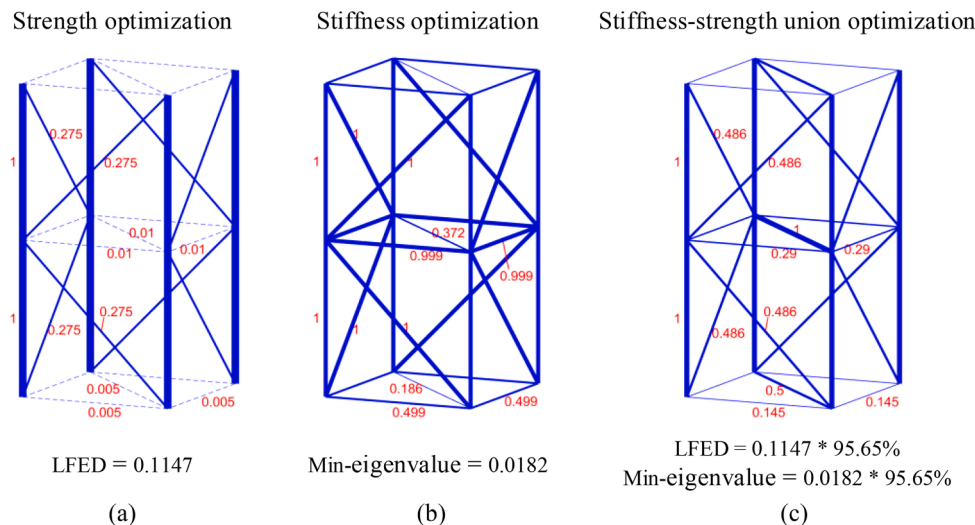


**Fig. 18.** Optimization results of a unit cell of a tower crane structure: (a) comprehensive strength optimization, (b) comprehensive stiffness optimization, and (c) synergistic optimization of the comprehensive strength and comprehensive stiffness, each reaching 95.65 % of the optimal values obtained from individual optimizations.

## **6. Conclusions and discussion**

This work is dedicated to establishing an index to evaluate and optimize the comprehensive strength of periodical structures. The conclusions can be summarized as follows:

- (1) The least failure energy density (LFED) is proposed as an index to evaluate the comprehensive strength of heterogeneous periodic structures and is applied to optimize both classical and new structures.
  - (2) The optimization of the LFED is essentially a two-layer nested optimization model, which is extremely demanding computational power. We find an analytical approach to compute LFED very quickly, which therefore turns the problem into a single-layer optimization model, reducing computational effort and enabling topological optimization of the problem.
  - (3) The upper bound of the LFED is found to be  $\frac{1}{6}\rho\frac{\sigma_c^2}{E}$  for 2D truss structures and  $\frac{1}{12}\rho\frac{\sigma_c^2}{E}$  for 3D truss structures.
  - (4) Through topology optimization based on the LFED, the optimal plane structure is found to be a curved-edge kagome structure, which is consistent with previous knowledge.
  - (5) Interestingly, rarely discussed space kagome structures (plate or lattice) are obtained through topological optimization via LFED, with a superior LFED and comprehensive strength compared with those of other classical structures.
  - (6) The concept of the LFED can be applied to the optimization of structures under other nonperiodic loads, such as beam structures and plate structures, which further demonstrates the wide applicability of the LFED.

Importantly, the current limitations on computational power restrict the grid size to approximately  $50 \times 50 \times 50$ . However, with more advanced computing power in the future, it is possible to further refine the grid and potentially discover even better-performing structures. The concept of LFED has applicability beyond heterogeneous periodic structures and can be applied to other materials, such as composites. Moreover, the method is fully applicable to the strength optimization of nonperiodic structures under infinite combinations of multiple basic loadings.

## CRediT authorship contribution statement

**Huawei Feng:** Writing – review & editing, Writing – original draft, Visualization, Validation, Software, Methodology, Investigation, Formal analysis, Conceptualization. **Peidong Lei:** Writing – review & editing, Visualization, Formal analysis. **Huikai Zhang:** Writing – review & editing, Formal analysis, Conceptualization. **Bin Liu:** Writing – review & editing, Supervision, Funding acquisition, Formal analysis, Conceptualization.

### **Declaration of competing interest**

The authors declare that they have no known competing financial interests or personal relationships that could have appeared to influence the work reported in this paper.

## Data availability

Data will be made available on request.

## Acknowledgments

This work was supported by the National Natural Science Foundation of China [grant numbers: 11720101002, 11921002, and 11890674].

## Supplementary materials

Supplementary material associated with this article can be found, in the online version, at [doi:10.1016/j.jmps.2024.105892](https://doi.org/10.1016/j.jmps.2024.105892).

## Appendix: Discussions on the upper bound of the LFED for truss structures

In the previous section, we observed that the optimized truss structures in 2D and 3D reach the upper bounds of LFED  $\frac{1}{6}\rho\frac{\sigma_c^2}{E}$  and  $\frac{1}{12}\rho\frac{\sigma_c^2}{E}$ , respectively. In this appendix, we aim to interpret this observation by assuming that all the struts are uniformly distributed (Gent and Thomas, 1963), as shown in Fig. A1, and then superimposing their stiffness matrices (Christensen, 1986).

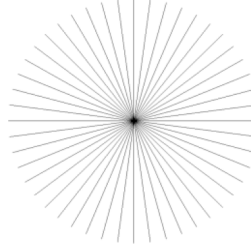


**Fig. A1.** Uniformly distributed struts.

When there are  $n$  ( $n \geq 3$ ) struts in the plane, which are equally distributed with an angle of  $\theta^{(i)} = \frac{i\pi}{n}$ , the corresponding stress and strain rotation matrices are

$$T_e^{(i)} = \begin{bmatrix} \cos(\theta)^2 & \sin(\theta)^2 & -\sin(\theta)\cos(\theta) \\ \sin(\theta)^2 & \cos(\theta)^2 & \sin(\theta)\cos(\theta) \\ 2\sin(\theta)\cos(\theta) & -2\sin(\theta)\cos(\theta) & \cos(\theta)^2 - \sin(\theta)^2 \end{bmatrix} \quad (\text{A1a})$$

$$T_\sigma^{(i)} = \begin{bmatrix} \cos(\theta)^2 & \sin(\theta)^2 & -2\sin(\theta)\cos(\theta) \\ \sin(\theta)^2 & \cos(\theta)^2 & 2\sin(\theta)\cos(\theta) \\ \sin(\theta)\cos(\theta) & -\sin(\theta)\cos(\theta) & \cos(\theta)^2 - \sin(\theta)^2 \end{bmatrix} \quad (\text{A1b})$$

The stiffness matrix of strut # $i$  is expressed as follows:

$$C^{(i)} = \frac{\rho E}{n} \begin{bmatrix} 1 & 0 & 0 \\ 0 & 0 & 0 \\ 0 & 0 & 0 \end{bmatrix} \quad (\text{A2})$$

By superimposing all the stiffness matrices, the overall stiffness matrix of the assembly can be estimated as follows:

$$C_* = \sum_{i=1}^n T_\sigma^{(i)} C^{(i)} T_e^{(i)^{-1}} = \frac{\rho E}{8} \begin{bmatrix} 3 & 1 & 0 \\ 1 & 3 & 0 \\ 0 & 0 & 1 \end{bmatrix} \quad (\text{A3})$$

which is isotropic.

If we take the Young's modulus of the strut material as  $E$ , then the Young's modulus of the structural stiffness matrix is  $\frac{E\rho}{3}$ , and Poisson's ratio is  $\frac{1}{3}$ ; subsequently, when we pull any one of the directional struts until it breaks, the strain energy density corresponding to the structure will be exactly  $\frac{1}{6}\rho\frac{\sigma_c^2}{E}$ .

Similarly, if an infinite number of struts are evenly distributed in space, then the overall stiffness matrix can be obtained as an isotropic stiffness matrix:

$$\mathbf{C} = \frac{E\rho}{15} \begin{bmatrix} 3 & 1 & 1 & 0 & 0 & 0 \\ 1 & 3 & 1 & 0 & 0 & 0 \\ 1 & 1 & 3 & 0 & 0 & 0 \\ 0 & 0 & 0 & 1 & 0 & 0 \\ 0 & 0 & 0 & 0 & 1 & 0 \\ 0 & 0 & 0 & 0 & 0 & 1 \end{bmatrix} \quad (\text{A4})$$

where the Young's modulus of the structural stiffness matrix is  $\frac{E\rho}{6}$  and Poisson's ratio is  $\frac{1}{4}$ . If we pull any one of the directional struts until it breaks, then the strain energy density corresponding to the overall structure will be exactly  $\frac{1}{12}\rho\frac{\sigma_c^2}{E}$ .

However, this interpretation holds only for the ideal case of uniformly distributed struts. In practice, we find that for some structures with anisotropic stiffness, such as octets, the LFED can also reach the upper bound. Thus, further exploration is needed to fully prove the existence of this upper limit.

## References

- Al-Ketan, O., Lee, D.W., Rowshan, R., Al-Rub, R.K.A., 2020. Functionally graded and multi-morphology sheet TPMS lattices: design, manufacturing, and mechanical properties. *J. Mech. Behav. Biomed. Mater.* 102, 103520.
- Ashby, M.F., 2006. The properties of foams and lattices. *Math., Phys. Eng. Sci.* 364 (1838), 15–30.
- Atwal, P., Conti, S., Geihe, B., Pach, M., Rumpf, M., Schultz, R., 2012. On shape optimization with stochastic loadings. *Constrain. Optimizat. Optimal Control. Part. Different. Equat.* 215–243.
- Bauer, J., Hengsbach, S., Tesari, I., Schwaiger, R., Kraft, O., 2014. High-strength cellular ceramic composites with 3D microarchitecture. *Proceed. Nat. Acad. Sci.* 111 (7), 2453–2458.
- Berger, J., Wadley, H., McMeeking, R., 2017. Mechanical metamaterials at the theoretical limit of isotropic elastic stiffness. *Nature* 543 (7646), 533–537.
- Bonatti, C., Mohr, D., 2019. Mechanical performance of additively-manufactured anisotropic and isotropic smooth shell-lattice materials: simulations & experiments. *J. Mech. Phys. Solids.* 122, 1–26.
- Chatterjee, T., Chakraborty, S., Goswami, S., Adhikari, S., Friswell, M.I., 2021. Robust topological designs for extreme metamaterial micro-structures. *Sci. Rep.* 11 (1), 1–14.
- Christensen, R., 1986. Mechanics of low density materials. *J. Mech. Phys. Solids.* 34 (6), 563–578.
- Coelho, P.G., Barroca, B.C., Conde, F.M., Guedes, J.M., 2021. Minimization of maximal von Mises stress in porous composite microstructures using shape and topology optimization. *Struct. Multidisciplin. Optimiz.* 64 (4), 1781–1799.
- Cui, Q., Zhang, H., Pawar, S.S., Yu, C., Feng, X. and Qiu, S., 2022. Topology optimization for 3D-printable large-scale metallic hollow structures with self-supporting. *Deshpande, V.S., Fleck, N.A., Ashby, M.F., 2001. Effective properties of the octet-truss lattice material. J. Mech. Phys. Solids.* 49 (8), 1747–1769.
- Gent, A., Thomas, A., 1963. Mechanics of foamed elastic materials. *Rubber Chem. Technol.* 36 (3), 597–610.
- Gurtner, G., Durand, M., 2014. Stiffest elastic networks. *Mathemat., Phys. Eng. Sci.* 470 (2164), 20130611.
- Hanks, B., Berthel, J., Frecker, M., Simpson, T.W., 2020. Mechanical properties of additively manufactured metal lattice structures: data review and design interface. *Addit. Manuf.* 35, 101301.
- Hashin, Z., 1960. The elastic moduli of heterogeneous materials. (Vol. 9). US Department of commerce, office of technical services, Washington, DC.
- Helou, M., Kara, S., 2018. Design, analysis and manufacturing of lattice structures: an overview. *Int. J. Comput. Integr. Manuf.* 31 (3), 243–261.
- Messner, M.C., 2016. Optimal lattice-structured materials. *J. Mech. Phys. Solids.* 96, 162–183.
- Pan, C., Han, Y., Lu, J., 2020. Design and optimization of lattice structures: a review. *Appl. Sci.* 10 (18), 6374.
- Paulino, G.H., Silva, E.C.N., Le, C.H., 2009. Optimal design of periodic functionally graded composites with prescribed properties. *Struct. Multidisciplin. Optimiz.* 38, 469–489.
- Sigmund, O., 2000. A new class of extremal composites. *J. Mech. Phys. Solids.* 48 (2), 397–428.
- Symons, D.D., Hutchinson, R.G., Fleck, N.A., 2004. Actuation of the kagome double layer grid. Part I: prediction of performance of the perfect structure. *Submitt. J. Mech. Phys. Solids.*
- Vasiliev, V., Razin, A., 2006. Anisogrid composite lattice structures for spacecraft and aircraft applications. *Compos. Struct.* 76 (1–2), 182–189.
- Wang, H., Wan, Y., Li, Q., Liu, X., Yu, M., Zhang, X., Liu, Z., 2022. Multiscale design and biomechanical evaluation of porous spinal fusion cage to realize specified mechanical properties. *Biodes. Manuf.* 1–17.
- Watts, S., Tortorelli, D.A., 2017. A geometric projection method for designing three-dimensional open lattices with inverse homogenization. *Int. J. Numer. Methods Eng.* 112 (11), 1564–1588.
- Zhang, H.K., Wu, W.J., Kang, Z., Feng, X.Q., 2020. Topology optimization method for the design of bioinspired self-similar hierarchical microstructures. *Comput. Methods Appl. Mech. Eng.* 372, 113399.
- Zheng, X., Lee, H., Weisgraber, T.H., Shusteff, M., DeOtte, J., Duoss, E.B., Jackson, J.A., 2014. Ultralight, ultrastiff mechanical metamaterials. *Science* 344 (6190), 1373–1377.
- Zhou, M., Sigmund, O., 2017. On fully stressed design and p-norm measures in structural optimization. *Struct. Multidisciplin. Optimiz.* 56, 731–736.